Published in "Chemistry – A European Journal 20(26): 8062–8067, 2014"
which should be cited to refer to this work.

The Primary Steps in Excited-State Hydrogen Transfer: The Phototautomerization of *o*-Nitrobenzyl Derivatives

Tomáš Šolomek, Christian G. Bochet, and Thomas Bally*[a]

Abstract: The quantum yield for the release of leaving groups from *o*-nitrobenzyl "caged" compounds varies greatly with the nature of these leaving groups, for reasons that have never been well understood. We found that the barriers for the primary hydrogen-atom transfer step and the efficient nonradiative processes on the excited singlet and triplet surfaces determine the quantum yields. The excited-state barriers decrease when the exothermicity of the photoreaction increases, in accord with Bell–Evans–Polanyi principle, a tool that has never been applied to a nonadiabatic photoreaction. We further introduce a simple ground-state predictor, the radical-stabilization energy, which correlates with the computed excited-state barriers and reaction energies, and that might be used to design new and more efficient photochemical processes.

Introduction

The design of new efficient photochemical processes suffers from our inability to reliably predict the outcome of chemical reactions involving excited states.[1] Despite recent theoretical developments that led to understanding of the role of conical intersections in determining the selectivity and quantum yields of excited state reactions,[2] this role cannot easily be expressed in terms of a qualitative model, such as those that are well understood and broadly used to describe thermal processes, for example, the Bell–Evans–Polanyi (BEP) principle. This principle should be applicable to any set of adiabatic potential energy surfaces for a class of similar reactions, but to the best of our knowledge, the BEP principle has never been applied to actually tune the outcome of a photochemical reaction.[3]

Excited-state hydrogen transfer (ESHT), a process that stood at the origin of modern photochemistry,[2a] plays an essential role in the functionality of many chemical and biological systems. In particular, the phototautomerization of *o*-nitrobenzyl (*o*NB) derivatives **1**[4] results in a cascade of irreversible reactions that lead to the ejection of leaving groups (LGs) X (Scheme 1), a reaction that has found numerous applications in photoactivatable ("caged") compounds in chemistry,[5] biochemistry,[6] macromolecular[7] and neural sciences,[8] photolithography,[9] or the fabrication of DNA chips.[10]

It has been shown that photoexcitation of **1** is followed by rapid (ca. 100 fs) internal conversion to the lowest singlet excited state and subsequently to ESHT, through both the singlet and triplet manifolds leading to the formation of *aci*-nitro tautomers (*Z*)-**2** through a conical intersection from ^{1}**1**, or through the triplet diradical **3** formed from ^{3}**1**.[11] The barrier for retautomerization of (*Z*)-**2** back to **1** is relatively low, but in some solvents (MeOH, acetonitrile), the equilibration between (*Z*)- and (*E*)-**2** by proton exchange between the oxygen atoms competes effectively with this unproductive process that would decrease the quantum yield of LG release.[12] Then, decay of **2** obeys a single exponential rate law and ultimately leads to the rate-limiting and irreversible release of LG.

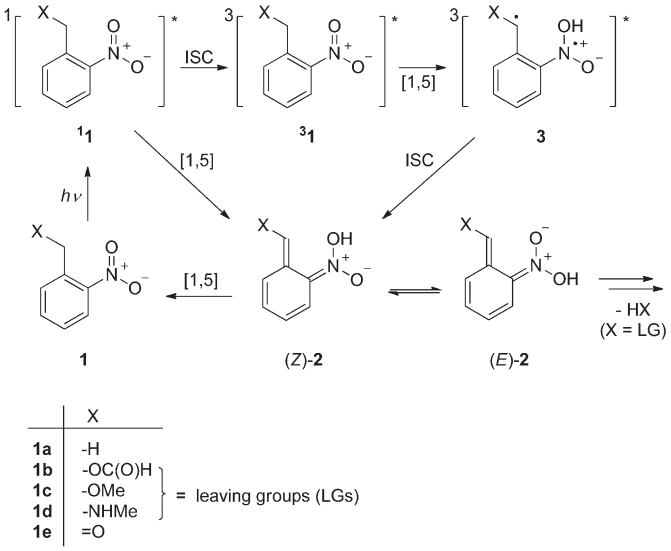

Scheme 1. Photochemistry of *o*-nitrobenzyl derivatives.

However, it was found that the quantum yields for the release of LGs from *o*NB derivatives depend strongly on the nature of the LG, and this limits their applicability to liberate certain LGs in a targeted fashion. Recently, we have shown that the quantum efficiency for the release of a LG correlates

[a] *T. Šolomek, Prof. Dr. C. G. Bochet, Prof. Dr. T. Bally*
Département de chimie, Université de Fribourg
Chemin du Musée 9, 1700 Fribourg (Switzerland)
E-mail: Thomas.Bally@unifr.ch

Supporting information for this article is available

with the radical stabilization energy (RSE) that this LG provides to *o*NB-type radicals (**4a** in Scheme 2).[13] We conjectured that radical-stabilizing groups must weaken the C–H bond that is being cleaved in the ESHT step and thus lower the excited-state barrier for this process and increase the overall quantum yield of the reaction.

Herein, we propose a model, based on quantum chemical calculations, that provides a general picture of ESHT reactions in **1**. Thereby, we aim to stimulate additional experimental work that is needed to fully understand the mechanism of this important photoreaction. Our model offers an explanation for why and how the quantum yields for the release of LGs from *o*NB derivatives depend on the nature of these LGs. We further demonstrate the validity of the BEP principle for the ESHT reaction in **1**, which makes that a simple ground-state predictor, the RSE,[13] correlates with the computed excited-state barriers and reaction energies and that this predictor might be used to design new and more efficient photochemical processes.

Table 1. Summary of calculated energies.[a]

	ΔE (S_1-S_0)[b] Vert.	Adiab.	ΔE (T_1-S_0)[c]	S_1 (nπ^*) barrier[d]	T_1 (nπ^*) barrier[e]	ΔE_S[f]	ΔE_T[e]	RSE[g]	QY[h]
1a	89.9	69.9	55.8	9.9 (10.5)	9.6	−38.8	−12.4	0.0	≈0.002[j]/≈0.08[k]
1b	89.7	74.1	56.1	6.5 (7.8)	7.1	−47.1	−18.2	5.1	0.0081[l]
1c	89.8	73.7	55.8	4.1 (5.0)	3.8	−50.4	−21.3	10.3	0.22[l]
1d	90.0	74.4	55.7	−0.7 (0.1)	−0.6	−55.6	−25.6	16.2	0.14[l]
1e	89.7	72.0	54.1	1.1 (−0.7)	0.0	−49.0	−16.5	≈16[j]	≈0.5[m]

[a] In kcal mol^{-1}, including zero point vibrational energies for all stationary points; the basis sets are specified in the Supporting Information. [b] MS-CASPT2 S_1-S_0 energy differences at BMK (vertical) and CASSCF (adiabatic) geometries. [c] Adiabatic difference of T_1 and S_0 energies calculated by the (U)BMK method. [d] $\Delta H_S^{\ddagger}$ at 0 K; MS-CASPT2 calculation; numbers in parentheses were calculated by the TD-M06-2X method. [e] $\Delta H_T^{\ddagger}$ at 0 K; UBMK calculation. [f] Calculated by a thermochemical cycle as the difference between the adiabatic $\Delta E(S_1-S_0)$ (footnote [b]) and the BMK ground state **1**→(*Z*)-**2** reaction energy. [g] Calculated according to the isodesmic reaction in Scheme 2 with the B2PLYP functional.[13] [h] Quantum yields of disappearance. [i] Not available by the current calculations; the estimate is based on the bond strengths reported in ref. [16]. [j] In water; adapted from ref[12a]. [k] Determined by picosecond transient absorption spectroscopy in THF, ref. [11d]; the discrepancy between the two numbers may arise from the different excitation wavelengths used in the two experiments. [l] Measured in acetonitrile for a related series of nitroveratryl caged compounds with leaving groups that chemically represent those considered in our current work. See ref. [13] for details. [m] Various solvents; adapted from refs. [14a] and [14b].

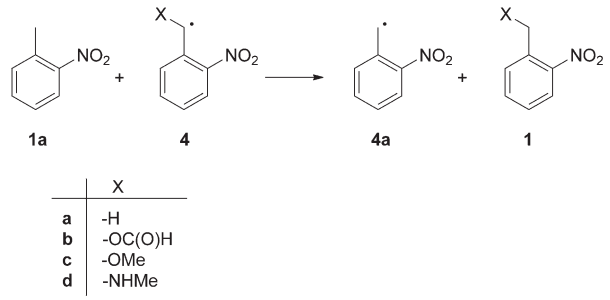

Scheme 2. Model reaction to evaluate relative C–H bond strengths by using the radical-stabilization energy (RSE).

Results and Discussion

We explored the lowest excited state potential energy surfaces that connect **1** to **2** by multireference MS-CASPT2 and by TD-DFT calculations for the singlet states, and by DFT calculations for the triplet states, for a series of *o*NB compounds **1a**–**d** (Scheme 1). *o*-Nitrobenzaldehyde (**1e**), a related and thoroughly studied system,[14] was used to validate the methods we applied in our present study. Derivatives **1b**–**d** represent molecules with typical leaving groups used in *o*NB-based "caged" compounds. They span a considerable range of quantum yields for their photodecomposition, and of the stabilization they provide to a radical center (see ref. [13]). The latter was estimated on the basis of RSEs (Table 1), which were calculated by using the isodesmic reaction shown in Scheme 2, with **1a** as the reference compound.[15]

The MS-CASPT2 method was shown to describe the excited singlet potential energy surfaces of *o*-nitrobenzaldehyde **1e** accurately;[14c,f] we reproduced the energies of important stationary points on the lowest singlet excited state (S_1) of **1e**. The TD-DFT approach was tested as an economical alternative to complement the multireference description of the S_1 surface and to provide zero point vibrational energy corrections to stationary points (see the Experimental Section). For the triplet states, DFT calculations with the BMK functional proved to provide predictions in accord with results of MS-CASPT2 method.

The lowest singlet excited state (S_1) of **1** can be described as resulting from an ^{1}nπ^* excitation that is localized mostly on the nitro group (see the Supporting Information). At the ground-state equilibrium geometry, the corresponding ^{3}nπ^* state lies between the above-described ^{1}nπ^* S_1 and the $^3\pi\pi^*$ excited state (Figure 1). Upon geometry relaxation, these two triplet states cross and the ^{3}nπ^* state becomes the lowest energy triplet state (T_1) at its equilibrium geometry.

Because the excitation is localized on the nitro group, the substituents X barely influence the energies of the three excited states, even after geometry relaxation to their respective energy minima (see $\Delta E(S_1-S_0)$ and $\Delta E(T_1-S_0)$ in Table 1). The picture changes markedly when the system begins to progress along the ESHT reaction coordinate: the energies of the singlet and triplet nπ^* states level off until a transition state is reached in both spin states, whereas the energy of the $^3\pi\pi^*$ state (now T_2) increases and crosses the S_1 surface before the ESHT transition state is reached. In the S_1 state, the radical character of the benzylic carbon increases until the system reaches the S_1/S_0 conical intersection, after passing the ESHT transition state, in which it returns to a closed-shell state that leads either to the *aci*-nitro intermediate (*Z*)-**2** or back to the starting nitro compound **1** (see Figure 1). After passing its own transition

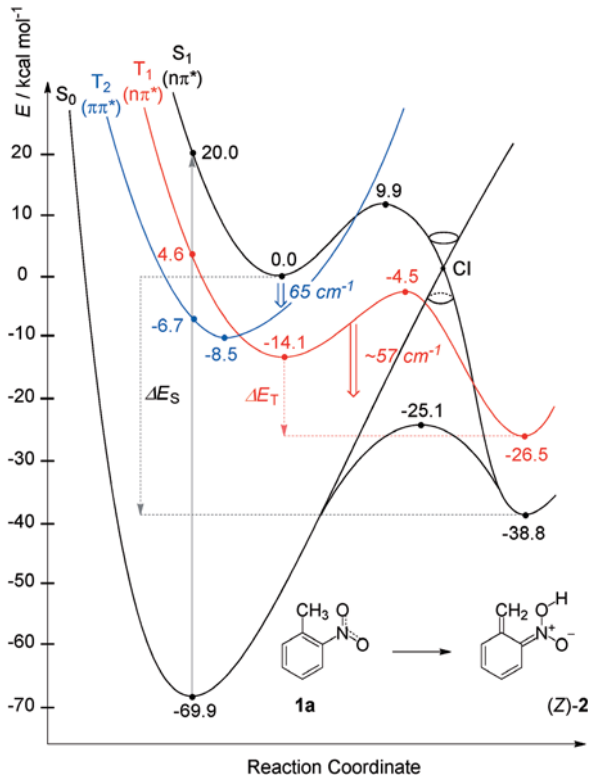

Figure 1. Singlet and triplet potential energy surfaces along the ESHT coordinate. Spin–orbit coupling values are given in italic.

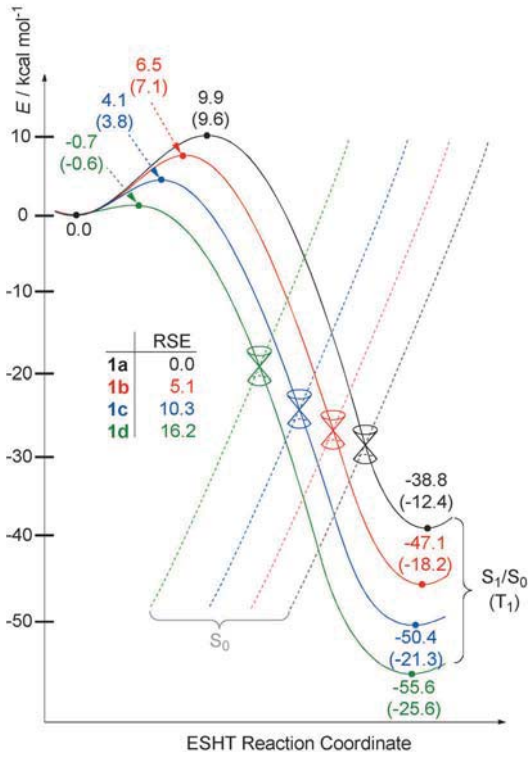

Figure 2. Singlet and triplet potential energy surfaces along the ESHT coordinate.

state, the triplet state relaxes to the fully diradicaloid structure **3** prior to intersystem crossing (ISC) and decay to **2**.

The coupling of the NO_2 chromophore and X through the benzyl-radical center that evolves along the ESHT reaction coordinate affects the shapes and the relative energies of the excited and ground-state energy surfaces along this coordinate (Figure 2). The barriers for ESHT calculated on the S_1 and T_1 surfaces by MS-CASPT2, TD-DFT, and DFT methods, respectively, are summarized in Table 1. Both sets of barriers depend strongly on the substituent X, but they are comparable in magnitude on the S_1 and the T_1 surfaces, which underlines the similarity of the electronic structure of these two states. The stabilization that a group X provides to the benzylic radical expresses itself in a lowering of the ESHT barrier, and the two quantities are in fact directly proportional (Figure 3). The overall reaction energies follow a similar trend with a strong increase of the exothermicity for good radical stabilizers (Figure SI1 in the Supporting Information).

Thus, the ESHT reaction of **1a–d** clearly follows the Bell–Evans–Polanyi principle both on the nonadiabatic S_1 and the adiabatic T_1 surfaces (see Figure 2). Remarkably, the position of the S_1/S_0 conical intersection points also varies with substituents, that is, the lengths of the forming O–H and the breaking C–H bonds involved in the ESHT are not the same at the S_1/S_0 intersection points for **1a–d**.

Their correlation with the RSE is depicted in Figure 4. The changes of the excited-state energy surfaces caused by substituents X determine the reactivity of ESHT. The NHMe substituent in **1d**, which acts as excellent radical-stabilizing group, diminishes the ESHT barrier in both the S_1 and the T_1 states to the extent that the process becomes nearly barrierless.

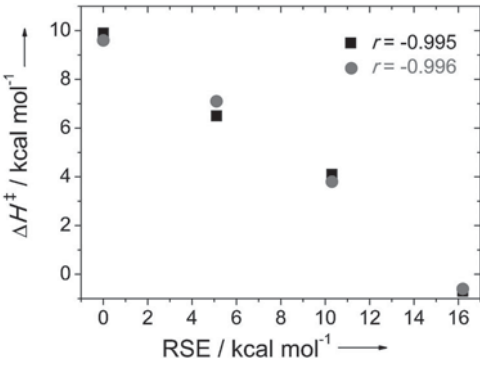

Figure 3. Correlation of RSE and S_1 (black squares)/T_1 (red circles) activation barrier for ESHT; Pearson's correlation coefficients are shown.

The branching ratio at the conical intersection then determines the quantum yield for the ultrafast formation of **2** (and hence for the LG release). In fact, the experimental quantum yield of approximately 0.5 for the decomposition of **1e**, which also has a nearly barrierless ESHT, has been reproduced quite well by nonadiabatic quantum-classical dynamics.[14d]

For derivatives, such as **1a–c**, which have energy barriers that prolong the S_1 lifetime, intersystem crossing becomes the major competing decay channel. Our calculations showed that the T_2 ($^3\pi\pi^*$) surface, which crosses the S_1 ($^1n\pi^*$) surface before

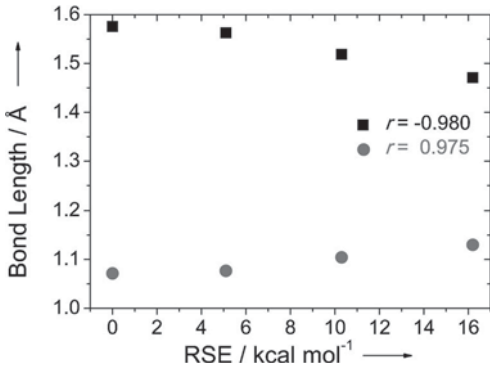

Figure 4. Correlation of RSE and selected bond lengths involved in the reaction coordinate of 1a–d at S_1/S_0 conical intersection (in Å; black squares: C–H, red circles: O–H); Pearson's correlation coefficients are shown.

the ESHT transition state is reached (blue line in Figure 1), acts as the primary "receiver state". The spin–orbit coupling (SOC) constants calculated for selected geometries on the S_1 surface for **1a–d** are as large as 65 cm^{-1} and confirm previous reports on ultrafast ISC rates (<3 ps) observed for nitroaromatic compounds, rates that can even compete with ultrafast singlet ESHT (Tables SI5–SI8 in the Supporting Information).[17] Upon relaxation, the T_2 state crosses and thus decays to the "reactive" T_1 state (red line in Figure 1).

A striking observation is the magnitude of the SOC (ca. 57 cm^{-1}) between the T_1 and S_0 surfaces in **1a–d** that was computed along the IRC path to the triplet ESHT transition state. The group of Terazima has reported extremely rapid deactivation of the lowest triplet state of nitrotoluenes with triplet lifetimes of approximately 500–600 ps.[11c] The T_1/S_0 energy gap along the IRC path is large and similar in **1a–d** and remains nearly constant, until the vicinity of the T_1 ESHT transition state is reached (Figure SI2 in the Supporting Information). Here, the singlet surface steeply approaches and crosses the triplet surface. If we assume that the wavepacket resides mostly at the bottom of the T_1 potential energy well, this suggests that ISC is driven by the large SOC, and that its rate is of similar magnitude for the entire series **1**. It is apparently this T_1/S_0 ISC that depletes the "reactive" T_1 surface before the triplet ESHT transition state is reached, and thus decreases the overall quantum yield for the release of LGs. The triplet ESHT would then be the step which limits the quantum yield in *o*NB-based "caged" compounds with poor radical stabilizing LGs despite their nucleofugality.

However, note that the rate of ISC may be strongly affected near the vicinity of the T_1 ESHT transition state, in which it can become a determining factor, especially for derivatives that possess late transition states and thus a smaller T_1/S_0 energy gap (Figure SI2 in the Supporting Information). Additional experimental and theoretical work is required to resolve this ambiguity by providing more accurate activation barriers than those provided here and, if possible, absolute ESHT and ISC rate constants. Nevertheless, both the barrier height and ISC tend to decrease the overall quantum yields for LGs that are poor radical stabilizers.

The occurrence of both singlet and triplet ESHT in photoexcited **1** may explain the surprisingly high quantum yields for LGs, such as RO^-, that are moderate radical stabilizers. If the ESHT barrier on the S_1 surface is high enough to allow for efficient population transfer to the triplet state by ISC, the overall quantum yield may, in principle, be higher than that for derivatives with barrierless ESHT on the S_1 surface, in which the quantum yield is inevitably dictated by the branching ratio at the S_1/S_0 conical intersection. The reason is that the prolonged lifetime of the T_1 state (compared to the S_1 state) allows for more efficient ESHT when the reaction barrier is not too high. We had already noted previously that the quantum yield for the release of alcohols from a very popular *o*NB-based photoremovable protecting group (PPG), the *o*-nitroveratryl group, was >1.5 times higher than that measured for the release of an amine from the same PPG, despite the higher RSEs (and thus lower ESHT barriers) for amines when employed as LGs.[13]

The ultrafast dynamics of ESHT in *o*NB system can also be at the origin of the enigmatic wavelength-dependent kinetic isotope effect (KIE) that can reach values as large as 8.3 and that has found interesting applications in processes involving chromatic orthogonality.[18] A comparison of ESHT/ESDT (excited-state deuterium transfer) barriers, in which the benzylic carbon carries Hs or Ds is shown in Table SI4 in the Supporting Information. Because the barriers for ESDT are invariably higher than those for ESHT, the KIE increases when the excitation excess energy from the vertical excitation decreases, especially if that excess energy is commensurate with the ESHT/ESDT barrier, in accord with the experimental observations. Such behavior gains importance when a wavelength, which extends to the biologically benign visible-light region, near the absorption band origin of an *o*NB-based PPG, is used to effect LG release. The low amount of excess energy imparted onto the chromophore may then prove insufficient for singlet and possibly even the triplet ESDT for systems with all but the best radical-stabilizing LGs.

Conclusion

We proposed a general model for the photorearrangement of *o*NB derivatives, a model that accounts also for nonradiative processes that can decrease the QY of formation of **2**, graphically illustrated in Figure 5. Depending on the wavelength at which **1** is irradiated, the $^1n\pi^*$ (S_1) or a higher excited state (e.g., $^1\pi\pi^*$, S_2) is initially populated. In the latter case, internal conversion leads to the rapid decay to the $^1n\pi^*$ state, following Kasha's rule. A leaving group that acts as a very good radical-stabilizing group causes the barrier on the S_1 surface to be small, which results in ultrafast singlet ESHT. For excellent radical-stabilizing groups, such as the NHMe group in **1d**, the S_1-ESHT may become a barrierless process. The part of the population transferred to the triplet state by ISC is then very small (Figure 5, top).

After passing the barrier on the S_1 surface, a conical intersection is encountered, and the branching ratio at that intersection limits the QY for the formation of **2** from the S_1 state. Intermediate S_1 barriers, as was found for LGs, such as alcohol-

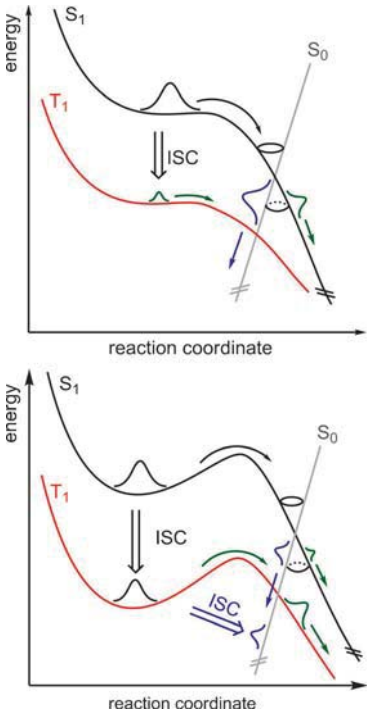

Figure 5. Fate of *o*-nitrobenzyl compounds that face low (top) or high (bottom) ESHT barriers in the S_1 and T_1 states (discussion, see Conclusion Section).The relative size of the wave packets denotes the contributions of different processes which increase (green) or decrease (blue) the quantum yield.

ates, prolong the lifetime of the S_1 state. In such cases, a part of the population in the S_1 state crosses the barrier and enters the conical intersection, whereas the remaining part is transferred to the $^3n\pi^*$ (T_1) state.

The lifetime of the $^3n\pi^*$ state of nitrobenzene is known to be approximately two orders of magnitude longer than that of the corresponding singlet excited state. Thus, there is more time to overcome essentially the same ESHT barrier that the reaction faced in the $^1n\pi^*$ state (Figure 5, bottom). Because there is no conical intersection in the triplet state, only a limited decrease of the QY is caused by the T_1/S_0 ISC and most of the molecules in the T_1 state decay to form the triplet diradical **3**, that is, **2** is formed with relatively small losses. Consequently, groups with intermediate RSEs that have moderate barriers can eventually have higher quantum yields than those with a nearly barrierless S_1 ESHT.

Finally, LGs that are poor radical-stabilizing groups face an impenetrable barrier in the $^1n\pi^*$ state, which causes most of the S_1 state population to be transferred to the T_1 state, where the competition between ESHT and T_1/S_0 ISC determines the QY. A rough estimation of the rate constant that corresponds to a barrier of approximately 7–10 kcal mol^{-1} suggests that the ESHT is rather inefficient in such cases.

We believe that the observations described in this paper can be generally applied to ultrafast photochemical processes, in which radical centers evolve during a photoreaction. In such cases, simple predictors, such as the RSE, can prove useful in guiding the design of new and more efficient photochemical processes beyond the particular case that we have examined here. In particular, a combination of substituents in both the benzylic position and the *o*-nitrophenyl ring in an *o*NB-based PPG that would lead to sufficient stabilization of the nascent radical center in ESHT should lead to increased quantum yields for release of even poor radical stabilizing LGs.

Methods

The DFT and TD-DFT calculations were performed with Gaussian 09 package of electronic-structure programs.[19] All geometry optimizations with CASSCF method, as well as spin–orbit coupling calculations, were carried out in a Molpro 2010 suite of electronic-structure programs,[20] whereas the single-point energy calculations employing perturbation theory to account for the dynamic electron correlation were carried out with MS-CASPT2 method and ANO-L-VTZP basis set with high-accuracy Cholesky decomposed two-electron integrals as implemented in Molcas 7.6.[21]

The ground and triplet state geometries were optimized with the (U)BMK functional that proved to describe the hydrogen-atom transfer reactions satisfactorily[22] and the 6-311+G(d,p) basis set. Frequency calculations were done to assess the stationary points and to provide zero point vibrational energies (ZPVEs). IRC calculations were used to check whether the transition states connected the desired energy minima. We took the advantage that the lowest $\pi\pi^*$ triplet state of **1a** belongs to C_s symmetry point group. The totally symmetric $^3A'$ wavefunction was computed and used to find the local energy minimum on the corresponding triplet surface. Otherwise, the SCF procedure led inherently to the lowest energy solution that can be described as an $n\pi^*$ triplet state when the symmetry was ignored.

Truhlar's M06-2X functional was shown to perform well for description of valence excited states, geometries of transition states for hydrogen transfer and overall thermochemistry[23] and was used for the TD-DFT calculations with 6-31G(d) basis set to complement the description of the S_1 energy surface by multireference theories (see below). Herein, the frequency calculations were performed at stationary points and the computed ZPVEs were then used to correct the energies obtained from the multireference MS-CASPT2 calculations. The ground-state energies on optimized S_1 surface stationary points were recomputed with the 6-311+G(3df,2p) basis set; electronic excitation energies from calculations with 6-31G(d) basis set were used.

The (10,9) active space (see Figures SI3–SI6 in the Supporting Information) was selected to perform the CASSCF geometry optimizations and transition-state searches with 6-31G(d) basis set. Two states were always averaged with equal weights. The CASSCF method does not describe the S_1 potential energy surface of **1** accurately and considerably overestimates the ESHT barrier.[14c,d,f] That is why we identified the stationary points of **1** on S_1 energy surface with MS-CASPT2 methodology as follows. We found that the CASSCF method led to artificial bending of the nitro group on both $n\pi^*$ S_1 and T_1 energy surfaces. The CAS(10,9) optimizations of S_1 energy minima of **1** by constraining the planar nitro group led to lowest energy geometries when MS-CASPT2/ANO-L-VTZP single-point energies were computed. These single-point calculations used the CASSCF/ANO-L-VTZP reference wavefunction with active space enlarged to (14,11) in the case of **1a**, **1c–d** and to (16,13) in the case of **1b** and **1e**. To obtain the geometries of transition state for the ESHT reaction, we first performed relaxed potential energy surface scans along the ESHT reaction coordinate (i.e., the C–H bond length), starting from from CAS(10,9)/6-31G(d) transition-

state structure, at the CAS(10,9)/6-31G(d) level of theory with step size of 0.0075 Å that gave a series of geometries that was subjected to MS-CASPT2/ANO-L-VTZP treatment with the CAS(10,9)/ANO-L-VTZP reference wavefunction. The point with the maximum energy obtained this way was considered as the transition state of ESHT. Its energy was then refined by MS-CASPT2/ANO-L-VTZP calculations by busing CASSCF reference wavefunctions with enlarged active space as was described above. The electronic energies were finally corrected by ZPVEs obtained from the TD-DFT calculations. It is gratifying to note that both the MS-CASPT2 energies obtained this way and the TD-DFT calculations are in very good agreement.

The S_1/S_0 conical intersection optimizations were performed at CAS(10,9)/6-31G(d) level of theory. The geometry was considered converged when the energy difference between the two intersecting surfaces was lower than 0.1 kcal mol^{-1}.

Spin–orbit coupling constants were calculated with CAS(10,9)/6-31G(d) wavefunctions with two singlet and two triplet states averaged with equal weights and by using the Breit–Pauli–Hamiltonian with one-center approximation used for one- and two-electron spin–orbit integrals as implemented in Molpro 2010 suite of electronic-structure programs).

Acknowledgements

We thank the Swiss National Science Foundation (grant No. 200020 143410) for its generous support of this work.

Keywords: Bell–Evans–Polanyi principle · hydrogen transfer · photochemistry · quantum chemical calculations · reaction mechanisms

[1] a) P. Štacko, T. Šolomek, P. Klán, *Org. Lett.* **2011**, *13*, 6556 – 6559; b) T. Šolomek, P. Štacko, A. T. Veetil, T. Pospíšil, P. Klán, *J. Org. Chem.* **2010**, *75*, 7300 – 7309 and references cited therein.

[2] a) P. Klán, J. Wirz, *Photochemistry of Organic Compounds: From Concepts to Practice*, John Wiley & Sons, Chichester, **2009**; b) F. Bernardi, M. Olivucci, M. A. Robb, *Chem. Soc. Rev.* **1996**, *25*, 321 – 328.

[3] There have been earlier attempts to relate the exothermicity of a photochemical reaction to its rate, see for example, H. E. Zimmerman, T. R. Welter, *J. Am. Chem. Soc.* **1978**, *100*, 4131 – 4145.

[4] P. Klán, T. Šolomek, C. G. Bochet, A. Blanc, R. Givens, M. Rubina, V. Popik, A. Kostikov, J. Wirz, *Chem. Rev.* **2013**, *113*, 119 – 191.

[5] L. Kammari, T. Šolomek, B. P. Ngoy, D. Heger, P. Klán, *J. Am. Chem. Soc.* **2010**, *132*, 11431 – 11433.

[6] G. C. R. Ellis-Davies, *Nat. Meth.* **2007**, *4*, 619 – 628.

[7] H. Zhao, E. S. Sterner, E. B. Coughlin, P. Theato, *Macromolecules* **2012**, *45*, 1723 – 1736.

[8] M. Goeldner, S. R. Givens, *Dynamic Studies in Biology*, Wiley-VCH, Weinheim, **2005**.

[9] a) U. Jonas, A. del Campo, C. Kruger, G. Glasser, D. Boos, *Proc. Natl. Acad. Sci. USA* **2002**, *99*, 5034 – 5039; b) V. San Miguel, C. G. Bochet, A. del Campo, *J. Am. Chem. Soc.* **2011**, *133*, 5380 – 5388.

[10] M. C. Pirrung, *Angew. Chem.* **2002**, *114,* 1326 – 1341; Angew. Chem. Int. Ed. **2002**, 41, 1276 – 1289.

[11] a) R. W. Yip, D. K. Sharma, R. Giasson, D. Gravel, *J. Phys. Chem.* **1984**, *88*, 5770 – 5772; b) R. W. Yip, D. K. Sharma, R. Giasson, D. Gravel, *J. Phys. Chem.* **1985**, *89*, 5328 – 5330; c) M. Takezaki, N. Hirota, M. Terazima, *J. Phys. Chem. A* **1997**, *101*, 3443 – 3448; d) T. Schmierer, S. Laimgruber, K. Haiser, K. Kiewisch, J. Neugebauer, P. Gilch, *Phys. Chem. Chem. Phys.* **2010**, *12*, 15653 – 15664; e) J.-M. Mewes, A. Dreuw, *Phys. Chem. Chem. Phys.* **2013**, *15*, 6691 – 6698.

[12] a) M. Schwörer, J. Wirz, *Helv. Chim. Acta* **2001**, *84*, 1441 – 1458; b) Y. V. Il'ichev, J. Wirz, *J. Phys. Chem. A* **2000**, *104*, 7856 – 7870; c) Y. V. Il'ichev, *J. Phys. Chem. A* **2003**, *107*, 10159 – 10170.

[13] T. Šolomek, S. Mercier, T. Bally, C. G. Bochet, *Photochem. Photobiol. Sci.* **2012**, *11*, 548 – 555.

[14] a) M. V. George, J. C. Scaiano, *J. Phys. Chem.* **1980**, *84*, 492 – 495; b) S. Laimgruber, W. J. Schreier, T. Schrader, F. Koller, W. Zinth, P. Gilch, *Angew. Chem.* **2005**, *117*, 8114 – 8118; *Angew. Chem. Int. Ed.* **2005**, *44*, 7901 – 7904; c) V. Leyva, I. Corral, T. Schmierer, B. Heinz, F. Feixas, A. Migani, L. Blancafort, P. Gilch, L. Gonzalez, *J. Phys. Chem. A* **2008**, *112*, 5046 – 5053; d) V. Leyva, I. Corral, F. Feixas, A. Migani, L. Blancafort, J. Gonzalez-Vazquez, L. Gonzalez, *Phys. Chem. Chem. Phys.* **2011**, *13*, 14685 – 14693; e) T. Schmierer, G. Ryseck, T. Villnow, N. Regner, P. Gilch, *Photochem. Photobiol. Sci.* **2012**, *11*, 1313 – 1321; f) A. Migani, V. Leyva, F. Feixas, T. Schmierer, P. Gilch, I. Corral, L. Gonzalez, L. Blancafort, *J. Chem. Soc. Chem. Commun.* **2011**, *47*, 6383 – 6385.

[15] A. S. Menon, G. P. F. Wood, D. Moran, L. Radom, *J. Phys. Chem. A* **2007**, *111*, 13638 – 13644.

[16] L. Yu-Ran, *Comprehensive Handbook of Chemical Bond Energies*, CRC Press, Boca Raton FL (USA), **2007**.

[17] R. Morales-Cueto, M. Esquivelzeta-Rabell, J. Saucedo-Zugazagoitia, J. Peon, *J. Phys. Chem. A* **2007**, *111*, 552 – 557.

[18] a) A. Blanc, C. G. Bochet, *J. Am. Chem. Soc.* **2004**, *126*, 7174 – 7175; b) A. Blanc, C. G. Bochet, *Org. Lett.* **2007**, *9*, 2649 – 2651.

[19] Gaussian 09, Revision D.01, M. J. Frisch, G. W. Trucks, H. B. Schlegel, G. E. Scuseria, M. A. Robb, J. R. Cheeseman, G. Scalmani, V. Barone, B. Mennucci, G. A. Petersson, H. Nakatsuji, M. Caricato, X. Li, H. P. Hratchian, A. F. Izmaylov, J. Bloino, G. Zheng, J. L. Sonnenberg, M. Hada, M. Ehara, K. Toyota, R. Fukuda, J. Hasegawa, M. Ishida, T. Nakajima, Y. Honda, O. Kitao, H. Nakai, T. Vreven, J. A. Montgomery, Jr., J. E. Peralta, F. Ogliaro, M. Bearpark, J. J. Heyd, E. Brothers, K. N. Kudin, V. N. Staroverov, R. Kobayashi, J. Normand, K. Raghavachari, A. Rendell, J. C. Burant, S. S. Iyengar, J. Tomasi, M. Cossi, N. Rega, J. M. Millam, M. Klene, J. E. Knox, J. B. Cross, V. Bakken, C. Adamo, J. Jaramillo, R. Gomperts, R. E. Stratmann, O. Yazyev, A. J. Austin, R. Cammi, C. Pomelli, J. W. Ochterski, R. L. Martin, K. Morokuma, V. G. Zakrzewski, G. A. Voth, P. Salvador, J. J. Dannenberg, S. Dapprich, A. D. Daniels, Ö. Farkas, J. B. Foresman, J. V. Ortiz, J. Cioslowski, D. J. Fox, Gaussian, Inc., Wallingford CT, 2009.

[20] MOLPRO, H.-J. Werner, P. J. Knowles, G. Knizia, F. R. Manby, M. Schütz, P. Celani, T. Korona, R. Lindh, A. Mitrushenkov, G. Rauhut, K. R. Shamasundar, T. B. Adler, R. D. Amos, A. Bernhardsson, A. Berning, D. L. Cooper, M. J. O. Deegan, A. J. Dobbyn, F. Eckert, E. Goll, C. Hampel, A. Hesselmann, G. Hetzer, T. Hrenar, G. Jansen, C. Köppl, Y. Liu, A. W. Lloyd, R. A. Mata, A. J. May, S. J. McNicholas, W. Meyer, M. E. Mura, A. Nicklaß, D. P. O'Neill, P. Palmieri, K. Pflüger, R. Pitzer, M. Reiher, T. Shiozaki, H. Stoll, A. J. Stone, R. Tarroni, T. Thorsteinsson, M. Wang, A. Wolf, 2010.1 ed., Cardiff, UK, **2010**.

[21] F. Aquilante, L. De Vico, N. Ferré, G. Ghigo, P.-Å. Malmqvist, P. Neogrády, T. B. Pedersen, M. Pitonak, M. Reiher, B. O. Roos, L. Serrano-Andrés, M. Urban, V. Veryazov, R. Lindh, *J. Comput. Chem.* **2010**, *31*, 224.

[22] J. Zheng, Y. Zhao, D. G. Truhlar, *J. Chem. Theory Comput.* **2007**, *3*, 569 – 582.

[23] X. Xu, I. M. Alecu, D. G. Truhlar, *J. Chem. Theory Comput.* **2011**, *7*, 1667 – 1676.